Structure and Function Analysis of Peptide Antagonists of Melanoma Inhibitor of Apoptosis (ML-IAP)‡

Matthew C. Franklin,§ Saloumeh Kadkhodayan,|| Heidi Ackerly,§ Daniela Alexandru,§ Mark D. Distefano,§,⊥ Linda O. Elliott,|| John A. Flygare,# Grace Mausisa,|| David C. Okawa,# Danny Ong,§ Domagoj Vucic,▽ Kurt Deshayes,*,§ and Wayne J. Fairbrother*,§

Departments of Protein Engineering, Bioanalytical Research and Development, Bioorganic Chemistry, and Molecular Oncology, Genentech, Inc., One DNA Way, South San Francisco, California 94080

Received February 10, 2003; Revised Manuscript Received April 22, 2003

ABSTRACT: Melanoma inhibitor of apoptosis (ML-IAP) is a potent anti-apoptotic protein that is upregulated in a number of melanoma cell lines but not expressed in most normal adult tissues. Overexpression of IAP proteins, such as ML-IAP or the ubiquitously expressed X-chromosome-linked IAP (XIAP), in human cancers has been shown to suppress apoptosis induced by a variety of stimuli. Peptides based on the processed N-terminus of Smac/DIABLO can negate the ability of overexpressed ML-IAP or XIAP to suppress drug-induced apoptosis. Such peptides have been demonstrated to bind to the single baculovirus IAP repeat (BIR) of ML-IAP and the third BIR of XIAP with similar high affinities (∼0.5 μM). Herein, we use phage-display of naïve peptide libraries and synthetic peptides to investigate the peptide-binding properties of ML-IAP-BIR and XIAP-BIR3. X-ray crystal structures of ML-IAP-BIR in complex with Smac- and phage-derived peptides, together with peptide structure−activity-relationship data, indicate that the peptides can be modified to provide increased binding affinity and selectivity for ML-IAP-BIR relative to XIAP-BIR3. For instance, substitution of Pro3′ in the Smac-based peptide (AVPIAQKSE) with (2*S*,3*S*)-3-methylpyrrolidine-2-carboxylic acid [(3*S*)-methyl-proline] results in a peptide with 7-fold greater affinity for ML-IAP-BIR and about 100-fold specificity for ML-IAP-BIR relative to XIAP-BIR3.

The inhibitor of apoptosis (IAP)[1] proteins are major regulators of apoptosis that confer protection against diverse pro-apoptotic stimuli (*1*). IAPs were first identified in baculoviral genomes, where they function as suppressors of the host-cell death response during viral infection (*2*−*4*). Additional IAPs were discovered subsequently in both invertebrates and vertebrates (*5*−*16*). All members of the IAP family contain one to three copies of the baculovirus IAP repeat (BIR) motif, and several also contain a C-terminal RING finger motif. BIRs are ∼80-residue zinc-binding domains that are essential for the anti-apoptotic activity of the IAPs (*17*) due in some part to their ability to bind to and inhibit caspases. The best-characterized of eight human IAPs is the ubiquitously expressed X-chromosome-linked IAP (XIAP), which contains three BIR domains and a RING finger domain. The second BIR domain (BIR2) together with the immediately preceding linker region of XIAP inhibits active caspases-3 and -7 (*18*−*22*), while BIR3 is a specific inhibitor of caspase-9 activation (*23*−*25*). Melanoma IAP (ML-IAP; also known as Livin or KIAP), which is not detectable in most normal adult tissues but is strongly upregulated in melanoma cell lines, contains a single BIR domain that has also been demonstrated to bind and inhibit caspases-3, -7, and -9 (*14*−*16*, *26*).

The interactions between caspase-9 and XIAP-BIR3 or ML-IAP-BIR are mediated by the N-terminus of the small subunit of caspase-9, which becomes exposed after proteolytic processing of procaspase-9 (*25*−*27*). The exposed N-terminus of the small subunit of caspase-9 is homologous to the processed N-termini of natural antagonists of the IAPs that promote apoptosis by competing with the binding of the caspase to the BIR domains; these IAP antagonists include the mammalian proteins Smac/DIABLO and HtrA2/Omi, as well as their functional *Drosophila* homologues Reaper, Hid, Grim, and Sickle (*28*−*40*) (Figure 1). Structural studies have revealed that these N-terminal peptides bind in an extended conformation to a surface groove on the BIR domains (*27*, *38*, *41*−*43*). The different peptide/BIR domain complexes are stabilized by electrostatic interactions involving the amide groups of the N-terminal alanine residues of the peptides, as well as several intermolecular hydrogen

‡ The coordinates have been deposited with the RCSB Protein Data Bank with the following accession codes: ML-IAP-BIR/AVPIAQKSE complex, 1OXQ; ML-IAP-BIR/AEAVPWKSE complex, 1OXN; and ML-IAP−BIR/AEVVAVKSE complex, 1OY7.

* To whom correspondence should be addressed. (K.D.) Phone: (650) 225-2046. Fax: (650) 225-3734. E-mail: deshayes@gene.com. (W.J.F.) Phone: (650) 225-6372. E-mail: fairbro@gene.com.

§ Department of Protein Engineering.

|| Department of Bioanalytical Research and Development.

⊥ Present address: University of Minnesota, Twin Cities Campus, Minneapolis, MN 55455.

Department of Bioorganic Chemistry.

▽ Department of Molecular Oncology.

[1] Abbreviations: BIR, baculovirus IAP repeat; DIAP, *Drosophila* inhibitor of apoptosis; DTT, dithiothreitol; FAM, 5-carboxyfluorescein; Fmoc, 9-fluorenylmethoxycarbonyl; HPLC, high-pressure liquid chromatography; IAP, inhibitor of apoptosis; IPTG, isopropyl β-D-thiogalactoside; ML-IAP, melanoma inhibitor of apoptosis; PEG, poly(ethylene glycol); PMSF, phenylmethylsulfonyl fluoride; SSRL, Stanford Synchrotron Radiation Laboratory; XIAP, X-chromosome-linked inhibitor of apoptosis.

10.1021/bi034227t CCC: $25.00
Published on Web 06/17/2003

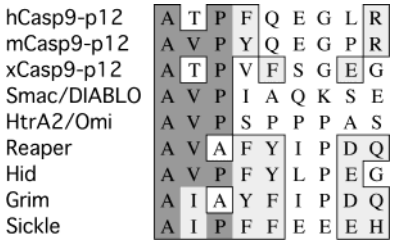

FIGURE 1: Amino acid sequence alignment of the nine N-terminal residues of the small subunit of active human, murine, and *Xenopus* caspase-9; active mammalian Smac/DIABLO and HtrA2/Omi; and *Drosophila* Reaper, Hid, Grim, and Sickle. Dark and light gray shading indicate identity and similarity, respectively.

bonds and hydrophobic interactions. Structural studies have shown also that the processed N-terminus of the small subunit of caspase-3 can contact the corresponding groove of XIAP-BIR2 (*22*), although mutation of Asp214 within this region to Ser or Ala does not affect the ability of XIAP to bind caspase-3 (*44*) or the ability of XIAP-BIR2 to inhibit caspase-3 (*19*). In contrast, the corresponding mutations in XIAP-BIR3 (Glu314Ser) and ML-IAP-BIR (Asp138Ala) significantly impair the binding of these proteins to both caspase-9 and Smac or Smac-based peptides (*24*, *26*, *41*, *44*).

Available peptide structure−activity-relationship (SAR) data for peptides binding to XIAP-BIR3 indicate that the binding affinity of the mature Smac protein is retained within its N-terminal four residues (*41*, *45*). Peptidomimetics or small molecules that also bind the tetrapeptide-binding site might therefore be useful therapeutics for the treatment of cancers that are resistant to pro-apoptotic drugs because of overexpression of IAPs. Indeed, we have shown recently that Smac-derived penetratin-fusion peptides are able to abrogate ML-IAP- and XIAP-mediated inhibition of adriamycin-induced apoptosis in MCF7 cells that are transiently transfected with either IAP (*26*). More recently, similar Smac-derived peptides were shown to sensitize a number of different tumor cell lines to apoptosis induced by death-receptor ligation or a variety of cytotoxic drugs (*46*−*48*). Furthermore, Smac-derived peptides were shown to enhance significantly the antitumor activity of Apo2L/TRAIL in an intracranial malignant glioma xenograft model in vivo (*48*).

In the present study, we explore the peptide-binding properties of ML-IAP by using phage display of naïve peptide libraries and in a more directed manner by using synthetic peptides containing natural and nonnatural amino acid substitutions at various positions. X-ray crystallographic structural analysis of Smac- and selected phage-derived peptides in complex with ML-IAP-BIR, together with the peptide SAR data, suggests regions of the peptides that could be modified to provide increased binding affinity and/or selectivity relative to XIAP.

MATERIALS AND METHODS

Protein Expression and Purification. Sequences encoding XIAP-BIR2 (amino acid residues 124−240 with mutations C202A and C213G) (*19*), XIAP-BIR3 (amino acid residues 241−356) (*24*), and ML-IAP-BIR (amino acid residues 63−179) were subcloned into pET15b vectors (Novagen) for bacterial expression. One liter cultures of *Escherichia coli* strain BL21 (DE3) transformed with vectors pET15b-XIAPBIR2C202AC213G, pET15b-XIAPBIR3, or pET15b-MLIAPBIR were induced with 1 mM isopropyl β-D-thiogalactoside (IPTG) for 4 h at 30 °C, pelleted, and resuspended in 100 mL of buffer containing 50 mM Tris [pH 8.0], 300 mM NaCl, 5 mM β-mercaptoethanol, 0.5 mM PMSF, 2 mM benzamidine, and 5 mM imidazole. Lysate produced by homogenization, microfluidization, and centrifugation was passed over Ni-NTA agarose (Qiagen) and Superdex 75 gel filtration (Pharmacia) columns, washed, eluted, and dialyzed against buffer containing 50 mM Tris (pH 8.0), 120 mM NaCl, 5 mM DTT, 0.5 mM PMSF, 2 mM benzamidine, 50 μM zinc acetate, and 1 mM sodium azide. Protein was concentrated and stored at −80 °C for further characterization.

Construction of Polyvalent Naïve Peptide-Phage Libraries. Libraries were constructed using methods described previously (*49*), with a phagemid vector containing an IPTG-inducible P_{tac} promoter driving the expression of open reading frames encoding fusion proteins containing the StII secretion signal (MKKNIAFLLASMFVFSIATNAYA), followed by 6, 8, 14, or 20 residue random peptides, a linker sequence (GGGSGGG), and the M13 gene-VIII major coat protein. Cleavage of the StII signal sequence in *E. coli* depends most strongly on the identities of the −3 and −1 residues, with Ala being preferred almost exclusively in these positions, while little preference is shown for residues downstream of the cleavage site (*50*).

Selection and Characterization of BIR-Binding Phage. Immunosorbant plates (Nunc Maxisorp) were coated with 5 μg/mL of BIR domain (ML-IAP-BIR, or XIAP-BIR2 or -BIR3) in 50 mM sodium carbonate buffer (pH 9.6) for 1 h at room temperature. The selection procedure used has been described previously (*51*). Individual phage clones from each round of selection were analyzed for specific binding to BIR domains using single-point phage ELISAs (*51*). Positive clones (those that bound to the BIR domain but not to BSA) were identified by sequencing DNA in a 96-well format as described (*51*).

Peptide Synthesis. Peptides were synthesized by either manual or automated (Milligen 9050) solid-phase synthesis at a 0.2 mM scale on PEG-polystyrene resin utilizing Fmoc chemistry. Purification was performed using HPLC with a H_2O-acetonitrile gradient with added 0.1% trifluoroacetic acid. Masses of each peptide were verified by electrospray mass spectrometry.

Peptide-Binding Assays. Polarization experiments were performed on an Analyst HT 96−384 (Molecular Devices Corp.). Samples for fluorescence polarization affinity measurements were prepared by addition of 1:2 serial dilutions of either ML-IAP-BIR, XIAP-BIR3, or XIAP-BIR2 in polarization buffer (50 mM Tris [pH 7.2], 120 mM NaCl, 1% bovine globulins, and 0.05% octylglucoside) to 5-carboxyfluorescein-conjugated peptides [AVPFAK(5-FAM)K (Hid-FAM) or AVPIAQKSEK(5-FAM) (Smac-FAM)] at 3−5 nM final concentrations. The reactions were read after an incubation time of 10 min at room temperature with standard cutoff filters for the fluorescein fluorophore (λ_{ex} = 485 nm; λ_{em} = 530 nm) in 96-well black HE96 plates (Molecular Devices Corp.). The apparent K_d values were determined from the EC_{50} values.

Competition experiments were performed by addition of ML-IAP-BIR, XIAP-BIR3, or XIAP-BIR2 proteins at 1, 1−2, or 30 μM, respectively, for Smac-FAM or 0.2, 0.5, or

30 μM, respectively, for Hid-FAM to wells containing probe as well as serial dilutions of the antagonists in the polarization buffer. Samples were read after a 10-min incubation. The inhibition constants (K_i) for the peptides were determined as described previously (*52*).

Crystallization and Data Collection. Peptides were reconstituted from lyophilized powder in 10 mM MES (pH 6.5). Peptides were added to ML-IAP-BIR protein (20 mg/mL in its storage buffer) in a 2:1 molar excess of peptide. The peptide/protein complex was mixed in a 1:1 ratio (total drop volume 2−4 μL) with well solution (50 mM sodium acetate [pH 5.0], 5% (v/v) PEG-300, 5 mM DTT) and equilibrated by vapor diffusion against the well solution. An immediate precipitate formed upon mixing, which gave rise to an oily, foamy skin in 1 day followed by growth of small rod-shaped crystals over the next week. Crystals also grew using ethanol, 2-propanol, or *tert*-butyl alcohol as precipitants; PEG-300 was preferred since it is the least volatile and worked well as a cryoprotectant. Crystals were separated from the skin of the crystallization drop and transferred to a stabilizer containing 50 mM sodium acetate (pH 5.0) and 10% (v/v) PEG-300, then transferred after 20 min to the same solution containing 20% PEG. After a further 20 min in the second cryostabilizer, the crystals were frozen in liquid nitrogen.

Cocrystallization trials were performed using the following peptides designed based on the results from the phage selection: AVPIAQKSE (Smac), AEAVPWKSE, AEAVAWKSE, AEVVAVKSE, AVGVPWKSE, AVPFAVKSE, AVPFYLKSE, AIPFEEKSE, and AEPWIGKSE. Of these, only the first four produced diffraction-quality crystals. Attempts to exchange one peptide for another by soaking the crystals were unsuccessful. We have not reported results for the AEAVAWKSE peptide because its diffraction quality and electron density maps were essentially identical to those of the AEAVPWKSE peptide (in both cases only the first four peptide residues were ordered).

Data for the MAD dataset (AEAVPWKSE peptide) were collected at beamline 9-2 of the Stanford Synchrotron Radiation Laboratory (SSRL). Data for the AVPIAQKSE peptide complex were collected by AXAS, Inc. on the COMCAT beamline (32IDB) of the Advanced Photon Source (Argonne, IL). Data for the AEVVAVKSE peptide complex were collected at SSRL beamline 1-5. Data were processed using HKL2000 (or DENZO and SCALEPACK separately (*53*)).

Structure Determination and Refinement. Molecular replacement with search models derived from BIR domain structures present in the Protein Data Bank was unsuccessful. MAD phasing, taking advantage of the anomalous scattering of the naturally bound zinc in the protein, was therefore used to solve the structure of the AEAVPWKSE peptide complex. The zinc sites were clearly evident in anomalous and dispersive Patterson maps calculated from the MAD data, and five sites were found using the Patterson search routine in CNX (Accelrys, Inc.). These sites were refined using CNX; however, MAD-phased maps at this stage were essentially uninterpretable. Density modification including solvent flipping (using CNX) produced easily interpretable density. The BIR2 domain of DIAP1 (residues 217−310; PDB accession code 1JD4) was then placed manually into density for each of the five copies of ML-IAP-BIR in the asymmetric unit and rigid-body refined. The amino acid sequence of the model was then changed to that of ML-IAP, and the resulting model was subjected to several rounds of simulated annealing, positional refinement, and individual atomic *B* factor refinement using CNX, interspersed with map inspection and model rebuilding (including building of the bound peptide) using O (*54*). The CCP4 suite of programs (*55*) (in particular, Refmac5 (*56*) and ARP/wARP (*57*)) was used for subsequent positional and *B* factor refinement, water picking, and the building and refinement of a heptaethylene glycol (PEG-330) molecule. Noncrystallographic symmetry restraints were not used at any point in the refinement.

Both of the AVPIAQKSE and AEVVAVKSE complex structures were sufficiently isomorphous with the MAD-phased data (cross *R* factors below 15%) that inspection of F_o(new peptide) − F_o(MAD peak wavelength) maps, phased using the refined AEAVPWKSE complex structure (without its peptide), clearly indicated what changes were required to the model to account for the new peptide. These changes (primarily substituting the new amino acids in the bound peptide and adjustment of the conformation of Lys121) were made, and the resulting model was put through one round of positional refinement and *B* factor refinement.

RESULTS

Selection of IAP-Binding Peptides. To ascertain the diversity of peptide sequences that bind to the BIR domains of ML-IAP and XIAP, multivalent M-13 phage libraries of linear peptides displayed on the gene-VIII phage coat protein were panned against ML-IAP-BIR, XIAP-BIR2, and XIAP-BIR3. Linear X_6, X_8, X_{14}, and X_{20} libraries were prepared and combined to give a library with 8×10^{10} members. A total of 96 individual clones were isolated for single-point phage ELISA analysis after four rounds of sorting against each protein target. The XIAP-BIR2 and -BIR3 sorts yielded clones that demonstrated strong binding to the BIR domains with no detectable binding to BSA. Sequencing revealed that 95% of the positive clones came from the X_6 and X_8 libraries, suggesting that the peptides were binding to localized epitopes in the protein domains.

In contrast, the initial ML-IAP selectants showed high BSA binding in almost all cases; sequencing identified binders consisting of primarily X_{20} peptides with a high proportion of hydrophobic residues. Since the peptides selected against the XIAP-BIR2 and -BIR3 were predominantly from the X_6 and X_8 sub-libraries, the X_{14} and X_{20} sub-libraries were not included in a subsequent combined library used for panning against ML-IAP-BIR. Following four rounds of selection using the new combined X_6 and X_8 libraries (4×10^{10} members), clones were isolated that bound to ML-IAP but not to BSA (Figure 2).

In these experiments, the actual diversities of the libraries (4×10^{10} unique clones) were greater than the theoretical diversities (2.5664×10^{10} unique natural peptide sequences) of the X_6 plus X_8 libraries. Thus, consensus sequences have been obtained from libraries that contain all possible amino acid combinations in the eight N-terminal positions. Similar sequences were obtained from sorts against both ML-IAP-BIR and XIAP-BIR3 (Figure 2). In both cases, Ala is the only residue observed at the N-terminus. Approximately 50% of the clones have Val in position 2′ (peptide residue numbers will hereafter be primed to distinguish them from protein

	Residue															
	1		2		3		4		5		6		7		8	
Target	AA	%	AA	%	AA	%	AA	%	AA	%	AA	%	AA	%	AA	%
XIAP-BIR2																
	A	98	E	45	A	51	V	65	D	13	W	41	A	13	A	23
	L	1	V	19	G	15	I	17	P	13	E	10	E	13	V	15
	S	1	T	12	V	11	D	2.8	G	12	G	8.2	W	13	W	15
			Q	11	C	6.2	E	2.8	V	9.2	D	8.2	I	13	I	15
			I	8.5	P	6.2	F	2.8	A	9.2	F	6.2	V	13	G	11
			D	4.3	K	3.1	G	2.8	L	7.9	V	5.2	M	13	L	10
			S	0.7	M	3.1	L	2.8	M	7.9	M	4.1	Q	6.5	P	3.8
					S	3.1	W	2.8	F	5.3	A	4.1	G	6.5	T	3.8
					R	1	A	1.4	W	5.3	P	3.1	L	4.3	S	2.5
									I	5.3	C	2.1	T	3.2		
									Q	2.6	L	2.1	S	2.2		
									S	2.6	S	2.1				
									E	2.6	Y	2.1				
									Y	2.6	T	1				
									T	1.3						
XIAP-BIR3																
	A	100	V	47	P	93	F	66	V	17	G	17	G	21	M	37
			M	9.7	A	3.7	W	12	A	16	E	16	A	16	G	26
			S	11	G	2.5	L	9	G	13	M	12	V	12	W	15
			T	6.1	V	1.2	I	6	M	13	V	12	E	8.2	F	7.3
			I	4.9			M	3	E	10	D	8.1	F	8.2	L	4.9
			L	4.9			V	3	L	7.6	A	6	I	8.2	A	3.7
			F	4.9			Y	1.5	F	6.3	T	5	M	8.2	T	3.7
			R	3.2					I	4.2	L	4.7	W	8.2	V	3.7
			A	2.4					N	4.2	S	4.7	P	4.1		
			E	2.4					T	3.1	F	4	L	2.7		
			Q	2.4					S	2.8	Q	4	S	2.7		
			G	1.2					Q	2.1	W	4				
									W	2.1	P	2				
ML-IAP-BIR																
	A	100	V	50	P	95	F	53	E	23	E	37	C	25	V	33
			I	20	V	5	W	32	G	19	L	15	W	26	E	28
			A	10			I	11	A	15	A	9.2	E	16	C	9.4
			T	10			M	5.3	I	15	G	9.2	V	12	M	9.4
			L	6.7					L	7.7	S	9.2	A	8.2	W	9.4
			S	3.3					M	7.7	D	9.2	F	8.2	P	4.7
									W	7.7	R	6.2	L	2.7	L	3.1
									V	3.8	T	4.6	S	2.7	S	3.1

FIGURE 2: Amino acid preferences (corrected for codon bias) for the binding peptides selected on phage against XIAP-BIR2, XIAP-BIR3, and ML-IAP-BIR. In each case, a total of 96 clones were sequenced.

residue numbers), and greater than 90% prefer Pro in position 3′. The fourth position exhibits a strong selection bias for aromatic hydrophobic residues with Phe being the most common and Trp the second most common residue. No obvious bias is observed for any other position, suggesting that the four N-terminal residues are the most important for BIR binding. The consensus sequence for both ML-IAP-BIR and XIAP-BIR3, AVPF, corresponds with the N-terminus of *Drosophila* Hid (Figure 1).

The results obtained from panning against XIAP-BIR2 differ significantly from those for ML-IAP-BIR and XIAP-BIR3. Although Ala is again highly conserved at the N-terminus, the acidic amino acid Glu is preferred at position 2′. The small hydrophobic residues Gly, Ala, and Val are selected at position 3′ in contrast to the almost exclusive selection of proline in this position for ML-IAP-BIR and XIAP-BIR3. In position 4′, the hydrophobic residues Val and Ile are favored over the larger aromatic amino acids found for ML-IAP-BIR and XIAP-BIR3.

Binding Affinities of Phage-Derived Peptides. To compare the relative affinities of the selected peptides for the different BIR domains, representative peptides were synthesized, and affinities were determined using a fluorescence polarization-based competition assay with a Smac-based 5-carboxyfluorescein-labeled peptide (Smac-FAM) as the probe (Table 1). As might be expected, the affinities of the phage-selected peptides for their target proteins are, in general, slightly greater than for the Smac-based peptide. Interestingly, the peptides selected for binding to XIAP-BIR2 exhibit at least 10-fold specificity for ML-IAP-BIR relative to XIAP-BIR3 (these peptides are on the order of 10-fold weaker than the

Table 1: K_i Values for Phage-Derived Peptides

protein target	selected phage-peptide sequence	K_i (μM) ML-IAP-BIR	XIAP-BIR3	XIAP-BIR2
a	AVPIAQKSE	0.5	0.67	13.8
ML-IAP BIR	AVPWGLKSE	0.42	0.54	6.9
ML-IAP BIR	AIPFEEKSE	0.44	0.59	8.7
ML-IAP BIR	AVPWIGKSE	0.33	0.56	13.3
XIAP-BIR3	AVPFAVKSE	0.16	0.39	14.7
XIAP-BIR2	AVGVPWKSE	6.0	>64	2.3
XIAP-BIR2	AEAVAWKSE	9.3	>64	2.5
XIAP-BIR2	ATAVIEKSE	4.3	>64	5.7
XIAP-BIR2	AEAVPWKSE	2.1	>64	3.6
XIAP-BIR2	AEVVAVKSE	4.4	>64	15
XIAP-BIR2	AQAVAWKSE	7	>64	4.2

[a] Smac-based control peptide. Other synthetic peptides correspond to six-residue phage-selected sequences appended with KSE at their C-termini to ensure peptide solubility.

Table 2: Data Collection and Refinement Statistics[a]

peptide	AVPIAQKSE	AEAVPWKSE MAD (Zn K edge)			AEVVAVKSE
data set		peak	inflection	remote	
wavelength (Å)	1.2686	1.2822	1.2834	1.1921	1.033
resolution (Å)	20−2.3	20−2.2	20−2.25	20−2.2	30−2.7
R_{sym}	6.5 (37.9)	4.0 (21.6)	5.0 (32.4)	5.0 (28.2)	13.7 (28.2)
$I/\sigma(I)$	21.8 (3.4)	19.1 (4.4)	14.2 (2.4)	14.9 (3.2)	8.5 (2.6)
redundancy	3.7 (3.9)	2.0 (2.0)	2.1 (2.1)	2.1 (2.1)	2.1 (2.1)
completeness	97.2 (100)	98.6 (99.6)	99.4 (99.8)	99.0 (99.8)	99.0 (99.5)
MAD phasing (Å)			20−3.0		
overall FOM			0.75		
refinement					
resolution range (Å)	20−2.3		20−2.2		20−2.7
unique reflections	59357		71265		32692
R_{cryst}[b]/R_{free}[c]	16.1/21.8		16.9/22.5		15.2/21.1
RMSD bonds (Å)	0.009		0.008		0.008
RMSD angles (deg)	1.07		1.02		1.08
Ramachandran statistics					
most favored (%)	86.8		86.6		86.1
additional allowed (%)	12.2		12.4		12.9

[a] The space group for all three structures is $P3_2$. The unit cell for the AVPIAQKSE structure is $a = 83.2$, $b = 83.2$, and $c = 93.6$ Å; the other two structures are approximately the same. Numbers in parentheses are statistics for the highest resolution shell. All data were scaled keeping Bijvoet mates separate. The AVPIAQKSE structure has five protein molecules in the asymmetric unit, with a total of 3998 protein atoms, 403 waters, 5 zinc atoms, and one heptaethylene glycol molecule. The other two structures have almost identical numbers of atoms. [b] $R_{cryst} = \sum|(F_{obs}) - (F_{calc})|/\sum(F_{obs})$. [c] R_{free} is defined similarly to R_{cryst} but comprises a test set of 5% of the total reflections that were not used in model refinement.

Smac-based peptide for binding to ML-IAP-BIR but more than 100-fold weaker for binding to XIAP-BIR3).

Structure of ML-IAP-BIR Bound to Smac- and Phage-Derived Peptides. To understand further the specificity differences observed for some of the phage-derived peptides, the BIR domain of ML-IAP was crystallized in complex with the Smac-based peptide (AVPIAQKSE) and with two different peptides that were selected for binding to XIAP-BIR2 (AEAVPWKSE and AEVVAVKSE). The structures were determined to resolutions between 2.2 and 2.8 Å (Table 2). All models have good geometry as assessed by PROCHECK (*58*). In each case, there are five copies of ML-IAP-BIR in the asymmetric unit of the crystals (Supporting Information Figure 1); the final atomic models contain protein residues 72−169 (protomer A), 72−171 (protomers B−D), and 78−171 (protomer E). Surprisingly, only one of the five BIR domains (protomer E) binds peptide in the Smac-binding pocket; the bound peptides have strong electron density for residues 1′−4′ and no density for the C-terminal five residues. Protomers A−D form a tetramer in which the Smac-binding pocket is occupied by residues Ala73−Thr74−Leu75−Ser76 from a neighboring protomer. A heptaethylene glycol molecule (one of two main species in PEG-300) further stabilizes this tetramer by interacting with a number of tyrosines at its center.

With the exception of the N-terminal region, which is disordered in the peptide-bound domain, and residues 116−119, which are found in two distinct conformations, the five BIR domains within each asymmetric unit are very similar with average backbone pairwise RMS deviations of ≤0.45 Å for superposition of residues 79−115 and 120−168. The BIR domain of ML-IAP comprises five α-helices, a three-stranded β-sheet, and a zinc atom chelated by three Cys and one His residues (Figure 3). The structures are thus similar to those of other peptide-bound BIR domains, including XIAP-BIR3/Smac (*42*), XIAP-BIR2/caspase-3 (*22*), and DIAP1-BIR2/Grim and Hid (*43*) complexes, with RMS deviations of <0.7 Å for all aligned Cα atoms.

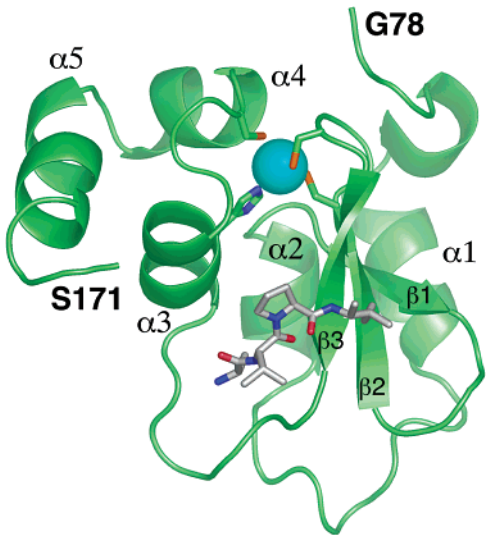

FIGURE 3: Overall structure of ML-IAP-BIR in complex with the Smac-based peptide AVPIAQKSE. The secondary structure comprises five α-helices (residues 87−92, 105−110, 140−147, 152−158, and 160−168) and a three-stranded β-sheet (residues 113−115, 122−124, and 130−132). Also shown is a zinc atom chelated by three Cys and one His residues (Cys124, Cys127, Cys151, and His 144). This figure was produced using the program PyMOL (*61*).

The binding interactions between ML-IAP−BIR and the Smac- and phage-derived peptides are essentially identical to those observed for Smac-derived peptides binding to XIAP-BIR3 (*41*, *42*), with only the N-terminal four residues of the peptide in contact with the protein (Figure 4). The N-termini of the peptides are in acidic environments with the amino group of Ala1′ hydrogen bonded to the side-chain carboxylates of Asp138 and Glu143. Peptide residues 2′−4′ form a highly twisted extension to the antiparallel β-sheet of ML-IAP-BIR, with hydrogen bonds between Val/Glu2′ amide and Gln132 carbonyl, Val/Glu2′ carbonyl and Gln132 amide, and a long (N−O distance ∼3.3 Å) hydrogen bond between Ile/Val4′ amide and Gly130 carbonyl. In the phage-derived peptide complexes, an additional hydrogen bond may

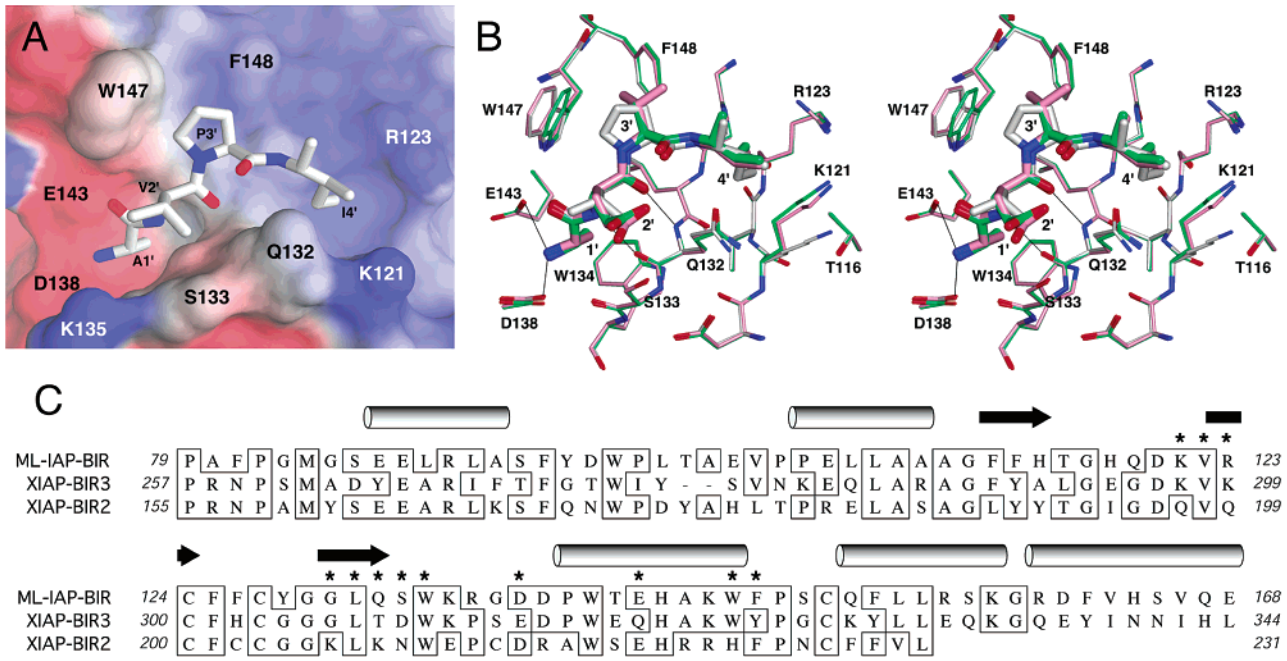

FIGURE 4: (A) Solvent-accessible surface representation of the peptide-binding site of ML-IAP-BIR color coded according to electrostatic surface potential: red, −10 kT; white, 0 kT; and blue, +10 kT. The bound Smac-based peptide is also shown. (B) Stereoview showing least-squares superpositions (using protein residues 78−170 and peptide residues 1′−4′) of the peptide-binding sites of complexes between ML-IAP-BIR and the peptides AVPIAQKSE (white carbon atoms), AEAVPWKSE (green), and AEVVAVKSE (pink). Hydrogen bonds between the peptide and the protein are indicated by thin lines. (C) Structure-based sequence alignment of ML-IAP-BIR, XIAP-BIR3, and XIAP-BIR2. The secondary structure of ML-IAP-BIR is indicated above the sequence. Residues indicated with an asterisk are within 4 Å of the Smac-based peptide in the ML-IAP-BIR/AVPIAQKSE complex structure. Panels A and B were produced using the program PyMOL (*61*).

be present between the side-chain carboxylate of Glu2′ and the side-chain hydroxyl of Ser133 (the Glu2′ side-chain is not as well-ordered as the rest of the peptide).

The interactions are further stabilized by hydrophobic contacts between the peptides and the ML-IAP-BIR. The methyl group of Ala1′ is buried in a hydrophobic pocket formed by the side chains of Leu131, Trp134, and Glu143. The side chain of peptide residue 2′ (Val/Glu2′) makes van der Waals contact with the β-methylene of Ser133 in each of the three complexes. Residue 3′ differs in the three complexes and makes different hydrophobic contacts in each case. Pro3′ in the Smac-derived peptide makes van der Waals contacts with Trp147 as well as the side chain of Val2′. The side-chain methyl of Ala3′ in the AEAVPWKSE peptide has no significant van der Waals contacts with the protein, while the side chain of Val3′ in AEVVAVKSE is readily accommodated in a hydrophobic groove defined by the side chains of Trp147 and Phe148. ML-IAP-BIR also tolerates Leu in this position of the peptide, as observed in the ML-IAP intermolecular interactions found in the crystal structures (Supporting Information Figure 1). Finally, the side chain of peptide residue 4′ (Ile/Val4′) interacts with a hydrophobic pocket defined by Gly130-Gln132 and the aliphatic portions of Thr116, Lys121, and Arg123. In the complexes with the phage-derived peptides, Lys121 has moved from its position in the Smac peptide complex to fill the space left vacant by substitution of Ile4′ with the smaller Val4′, indicating that there is some flexibility in this pocket.

Positional Scanning. The results of the phage sorting and subsequent structural analysis of the ML-IAP-BIR/peptide complexes suggest that peptide modifications could be made that would increase binding affinity and selectivity for ML-IAP relative to XIAP-BIR3. To examine the effects of substitutions at positions 2′, 3′, and 4′ in a more systematic manner, a series of single point mutants were synthesized in the background of the Smac-based peptide, AVPIAQKSE, and measured for binding to ML-IAP-BIR, XIAP-BIR3, and XIAP-BIR2. The Smac-based peptide was selected over the higher affinity peptides, AVPFAQKSE or AVPFAVKSE, as the background for these studies because binding to ML-IAP-BIR and XIAP-BIR3 was found to be significantly more sensitive to alanine substitutions at positions 2′ or 3′ when residue 4′ was an Ile rather than a Phe (see Supporting Information Table 1). The K_i values for the mutant peptides relative to the K_i of AVPIAQKSE binding to ML-IAP-BIR are plotted for ML-IAP-BIR and XIAP-BIR3 in Figure 5 (K_i values for peptides binding to ML-IAP-BIR, XIAP-BIR3, and XIAP-BIR2 are also reported in Supporting Information Table 1). The importance of these residues for binding to both ML-IAP-BIR and XIAP-BIR3 is emphasized by the greater than 10-fold losses in affinity observed upon substitution with Ala. Of the other natural amino acid substitutions tested, only Phe and Trp at position 4′ result in increased affinity relative to the Smac-based peptide. These results are consistent with the phage-display data that suggested the consensus sequence AVPF was optimal for binding to both BIR domains.

Several mutations result in improved specificity for ML-IAP-BIR relative to XIAP-BIR3. In particular, mutant peptides with Glu or Asp at position 2′ are 7−8-fold selective for ML-IAP-BIR (Figure 5A). Substitution of Pro3′ with either Val, Ile, or Leu results in greater than 10-fold specificity for ML-IAP-BIR (Figure 5B). Structure-based modeling (see Discussion) suggested that substitution of

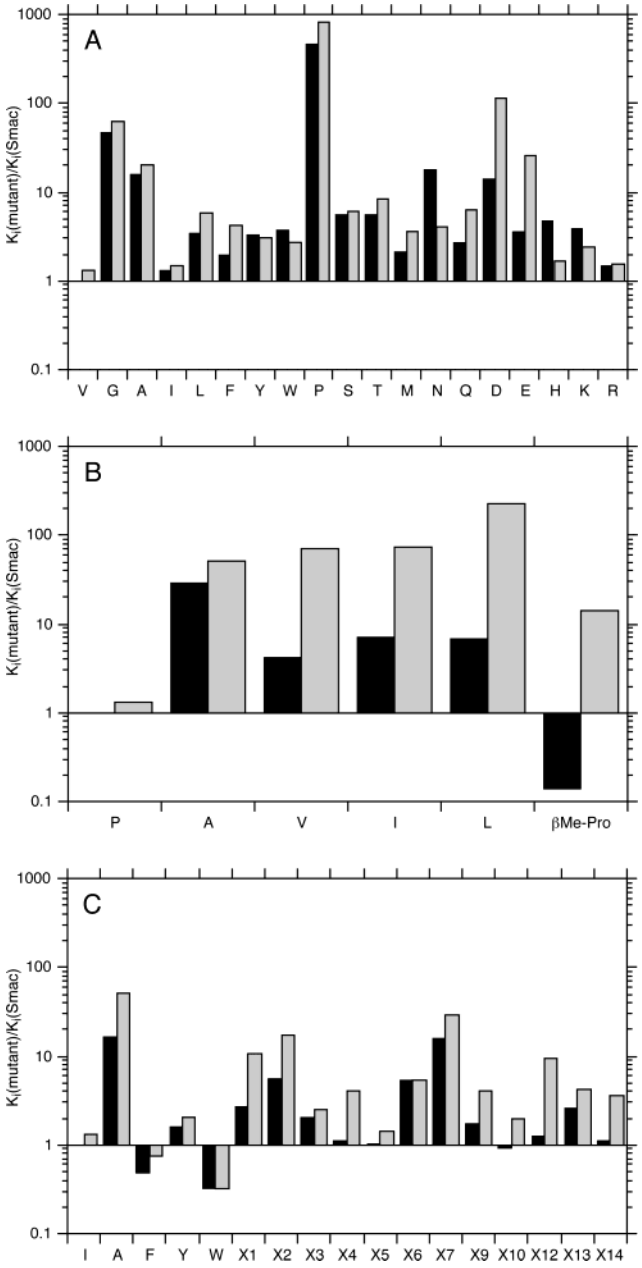

FIGURE 5: Log plots of relative K_i [K_i(mutant peptide/protein)/K_i(Smac peptide/ML-IAP-BIR)] for Smac-based peptides substituted at residues 2′ (A), 3′ (B), or 4′ (C) binding to ML-IAP-BIR (black) or XIAP-BIR3 (gray). K_i values were determined from a fluorescence polarization competition assay using either Smac-FAM or Hid-FAM probes (as described in the Materials and Methods). K_d values for these probes are 0.15 and 0.038 μM, respectively, for binding to ML-IAP-BIR and 0.26 and 0.11 μM, respectively, for binding to XIAP-BIR3. Nonnatural amino acids are indicated as follows: βMe-Pro, (3*S*)-methyl-proline; X1, 2-naphthylalanine; X2, phenylalanine-4-sulfonic acid; X3, 4-nitro-phenylalanine; X4, 4-amino-phenylalanine; X5, 3-methoxy-phenylalanine; X6, cyclohexylalanine; X7, cyclopentylalanine; X9, 3,5-dibromo-tyrosine; X10, 4-iodo-phenylalanine; X12, homophenylalanine; X13, 4-keto-phenyl-phenylalanine; and X14, 4-phenyl-phenylalanine.

Pro3′ with (2*S*,3*S*)-3-methylpyrrolidine-2-carboxylic acid [(3*S*)-methyl-proline] would result in a peptide with improved affinity for ML-IAP-BIR relative to the Val, Ile, or Leu substituted peptides, while maintaining the specificity advantage imparted by these amino acids. The resulting peptide has 7-fold greater affinity for ML-IAP-BIR than the starting Smac-based peptide (K_i = 70 nM as compared to 0.5 μM) and is ~100-fold specific for ML-IAP-BIR relative to XIAP-BIR3 (Figure 5B).

A number of nonnatural amino acid substitutions at position 4′ also result in improved specificity for ML-IAP-BIR. The greatest specificity enhancement is observed with homophenylalanine (X12) (~7-fold), followed by 2-naphthylalanine (X1), 4-amino-phenylalanine (X4), and 4-phenyl-phenylalanine (X14) (Figure 5C). Of these substitutions, only 2-naphthylalanine has a significantly reduced affinity for ML-IAP-BIR, relative to the Smac-based peptide (~3-fold reduced), while the binding affinity for XIAP-BIR3 is reduced in all four cases.

DISCUSSION

IAPs are frequently overexpressed in human cancers, and overexpression has been shown to suppress apoptosis induced by a variety of stimuli (*14*, *16*, *59*, *60*). Thus, IAP antagonists have obvious therapeutic potential in the treatment of cancers that resist conventional chemotherapeutic agents. XIAP, however, is expressed in most adult (and fetal) tissues examined (*8*, *9*); XIAP antagonists may, therefore, also sensitize normal cells to apoptosis induced by nonspecific cytotoxic drugs. In contrast, ML-IAP is not detectable in most normal adult tissues but is readily detected in a number of melanoma cell lines (*14*−*16*). Given that ML-IAP-overexpressing melanoma cell lines are more resistant to apoptotic stimuli than normal primary melanocytes (that do not express ML-IAP) (*14*), there may be utility in developing IAP antagonists that are specific for ML-IAP relative to XIAP.

Our phage-display data indicate that the optimal natural amino acid sequence for binding to both ML-IAP-BIR and XIAP-BIR3 corresponds to the N-terminus of the *Drosophila* IAP antagonist Hid (AVPF) (Table 1). Peptides based on the N-terminus of Hid have been shown previously to bind to XIAP-BIR3 somewhat tighter than Smac-based peptides (*41*, *43*, *45*), consistent with the observed preference for this sequence in the phage selection. The phage selection data also demonstrate, however, that ML-IAP-BIR is more tolerant of substitutions at peptide residues 2′, 3′, and 4′ than is XIAP-BIR3 (Table 1), suggesting that modifications of these peptide residues might result in increased selectivity for ML-IAP relative to XIAP. In contrast, the peptides derived from phage selection against XIAP-BIR2 showed decreased selectivity for ML-IAP relative to XIAP-BIR2 (Table 1). However, the mechanism of caspase-3 inhibition by XIAP-BIR2 as revealed by the crystal structure of the caspase-3/XIAP-BIR2 complex (*22*) and the observation that mutations in the Smac-peptide-binding site of XIAP-BIR2 do not impair its ability to inhibit caspase-3 (*19*, *44*) suggest that peptides or small molecules targeting this site would not be effective antagonists of XIAP-mediated caspase-3 inhibition. For this reason, we have chosen to focus our efforts on finding peptides with increased affinity and selectivity for ML-IAP-BIR relative to XIAP-BIR3.

The observation that ML-IAP-BIR is more tolerant of peptide substitutions than is XIAP-BIR3 was confirmed and extended by analysis of a series of single-point peptide mutants in which residues 2′, 3′, or 4′ were substituted with either natural or nonnatural amino acids. The peptide positional scanning data reported here for XIAP-BIR3 are in good general agreement with a recent similar study (*45*).

Small discrepancies that do exist may be due, in part, to differences in assay format and/or context dependence since the previous study used tetrapeptides, while in the current study the affinities of nine-residue peptides were compared. The positional scanning data for peptides binding to XIAP-BIR2 (Supporting Information Table 1) are significantly noisier than the corresponding data for ML-IAP-BIR and XIAP-BIR3 because of the lower affinity of the peptides, making these data more difficult to interpret. In contrast to both ML-IAP-BIR and XIAP-BIR3, however, none of the peptides tested had submicromolar K_i values for XIAP-BIR2.

Comparison of the structures of ML-IAP-BIR in complex with Smac- or phage-derived peptides with the available structures of XIAP-BIR3 in complex with Smac-based peptides suggests rational explanations for the observed specificity differences. For instance, an acidic residue at peptide position 2′ appears unfavorable for binding to XIAP-BIR3 because of its proximity to Asp309 in the peptide-binding site; in complex with ML-IAP-BIR, however, a Glu residue at position 2′ can form an additional hydrogen bond with the corresponding residue, Ser133 (Figure 4). In XIAP-BIR2, this residue is Asn209 that, together with the preceding residue, Lys208, likely provides favorable interactions with Glu2′ of the peptide, hence the selection for a Glu in the phage sorting.

ML-IAP-BIR has a hydrophobic groove formed by the side chains of Trp147 and Phe148 that can interact favorably with a γ-methyl group of either Val or Ile at peptide position 3′ (a Leu side chain can also interact with this site). Similar interactions are not possible with XIAP-BIR3 because of steric clashes with the hydroxyl moiety of Tyr324 (the residue corresponding to Phe148 in ML-IAP), resulting in 10−30-fold specificity for ML-IAP-BIR relative to XIAP-BIR3 when Pro3′ is substituted with Val, Ile, or Leu. Why XIAP-BIR2 prefers the small amino acids Gly, Ala, or Val over Pro in position 3′ is less clear, although these residues might permit the formation of a hydrogen bond between the peptide amide group and the side chain of His223 on the protein. Loss of Pro3′ results in loss of hydrophobic contact between the peptide and the corresponding residues in XIAP-BIR3 and ML-IAP-BIR (Trp323 and Trp147, respectively), without the possibility of introducing a new hydrogen bond. Consistent with the present data, previous studies have shown that the Pro3′Ala substitution reduces the binding affinity for XIAP-BIR3 by ∼50-fold while improving slightly the affinity for XIAP-BIR2 (*41*).

In general, it seems that both ML-IAP-BIR and XIAP-BIR3 prefer a Trp or Phe in position 4′, although ML-IAP-BIR is somewhat more tolerant of larger substituents, in particular para-substituted phenyl rings, than XIAP-BIR3. Indeed, the pocket of ML-IAP-BIR that binds peptide residue 4′ (P4′) is deeper than that of XIAP-BIR3 because of substitution of Leu292 in XIAP to Thr116 in ML-IAP.

Analysis of the interaction between peptide position 3′ and ML-IAP-BIR suggested that substitution of Pro3′ in the Smac-based peptide with (3*S*)-methyl-proline would improve the binding affinity for ML-IAP-BIR while decreasing affinity for XIAP-BIR3 because of the steric clash described above. Indeed, the modified peptide shows a 7-fold increase in affinity for ML-IAP-BIR and a 10-fold decrease in affinity for XIAP-BIR3, giving a selectivity for ML-IAP-BIR of ∼100. Affinity for XIAP-BIR2 is decreased by less than 2-fold, giving a selectivity for ML-IAP-BIR relative to XIAP-BIR2 of ∼300. Thus, relatively simple modifications, such as the addition of a single methyl group, can lead to significant improvements in both affinity and selectivity for ML-IAP-BIR. Structural analysis also indicates that ML-IAP-BIR has a slightly larger P4′-binding pocket than XIAP-BIR3, which may allow it to accommodate larger amino acid side chains; improved specificity for ML-IAP-BIR was in fact achieved by incorporation of larger nonnatural amino acids, such as homophenylalanine, at this position.

The structural and peptide SAR data presented here indicate that IAP-binding peptides can be modified to provide increased binding affinity and selectivity for ML-IAP-BIR relative to XIAP-BIR3 and XIAP-BIR2. These data will aid in the design of potent, ML-IAP-specific, peptidomimetics or small molecules that may be useful for the treament of cancers, in particular melanomas, in which ML-IAP expression contributes to resistance against conventional chemotherapeutic agents.

ACKNOWLEDGMENT

We thank Sachdev Sidhu for help with the peptide phage display experiments; Sarah Hymowitz, Christian Wiesmann, Charles Eigenbrot, Jennifer Stamos, and Mark Ultsch for help with X-ray data collection; and Bart de Vos and Melissa Starovasnik for helpful discussions.

SUPPORTING INFORMATION AVAILABLE

One figure showing five copies of ML-IAP-BIR in the asymmetric unit of the crystals and a stereoview of ML-IAP residues Gly72−Ser76 bound in the peptide-binding site of a symmetry related protein molecule, and one table listing the K_i values for positional scanning peptide homologues bound to ML-IAP-BIR, XIAP-BIR2, and XIAP-BIR3. This material is available free of charge via the Internet at http://pubs.acs.org.

REFERENCES

1. Salvesen, G. S., and Duckett, C. S. (2002) *Nat. Rev. 3*, 401−10.
2. Crook, N. E., Clem, R. J., and Miller, L. K. (1993) *J. Virol. 67*, 2168−74.
3. Birnbaum, M. J., Clem, R. J., and Miller, L. K. (1994) *J. Virol. 68*, 2521−8.
4. Clem, R. J., and Miller, L. K. (1994) *Mol. Cell. Biol. 14*, 5212−22.
5. Rothe, M., Pan, M. G., Henzel, W. J., Ayres, T. M., and Goeddel, D. V. (1995) *Cell 83*, 1243−52.
6. Roy, N., Mahadevan, M. S., McLean, M., Shutler, G., Yaraghi, Z., Farahani, R., Baird, S., Besner-Johnston, A., Lefebvre, C., Kang, X., Salih, M., Aubry, H., Tamai, K., Guan, X., Ioannou, P., Crawford, T. O., de Jong, P. J., Surh, L., Ikeda, J., Korneluk, R. G., and MacKenzie, A. (1995) *Cell 80*, 167−78.
7. Hay, B. A., Wassarman, D. A., and Rubin, G. M. (1995) *Cell 83*, 1253−62.
8. Duckett, C. S., Nava, V. E., Gedrich, R. W., Clem, R. J., Van Dongen, J. L., Gilfillan, M. C., Shiels, H., Hardwick, J. M., and Thompson, C. B. (1996) *EMBO J. 15*, 2685−94.
9. Liston, P., Roy, N., Tamai, K., Lefebvre, C., Baird, S., Cherton-Horvat, G., Farahani, R., McLean, M., Ikeda, J. E., MacKenzie, A., and Korneluk, R. G. (1996) *Nature 379*, 349−53.
10. Uren, A. G., Pakusch, M., Hawkins, C. J., Puls, K. L., and Vaux, D. L. (1996) *Proc. Natl. Acad. Sci. U.S.A. 93*, 4974−8.
11. Ambrosini, G., Adida, C., and Altieri, D. C. (1997) *Nat. Med. 3*, 917−21.

12. Fraser, A. G., James, C., Evan, G. I., and Hengartner, M. O. (1999) *Curr. Biol. 9*, 292−301.
13. Uren, A. G., Beilharz, T., O'Connell, M. J., Bugg, S. J., van Driel, R., Vaux, D. L., and Lithgow, T. (1999) *Proc. Natl. Acad. Sci. U.S.A. 96*, 10170−5.
14. Vucic, D., Stennicke, H. R., Pisabarro, M. T., Salvesen, G. S., and Dixit, V. M. (2000) *Curr. Biol. 10*, 1359−66.
15. Lin, J.-H., Deng, G., Huang, Q., and Morser, J. (2000) *Biochem. Biophys. Res. Commun. 279*, 820−31.
16. Kasof, G. M., and Gomes, B. C. (2001) *J. Biol. Chem. 276*, 3238−46.
17. Duckett, C. S., Li, F., Wang, Y., Tomaselli, K. J., Thompson, C. B., and Armstrong, R. C. (1998) *Mol. Cell. Biol. 18*, 608−15.
18. Takahashi, R., Deveraux, Q., Tamm, I., Welsh, K., Assa-Munt, N., Salvesen, G. S., and Reed, J. C. (1998) *J. Biol. Chem. 273*, 7787−90.
19. Sun, C., Cai, M., Gunasekera, A. H., Meadows, R. P., Wang, H., Chen, J., Zhang, H., Wu, W., Xu, N., Ng, S. C., and Fesik, S. W. (1999) *Nature 401*, 818−22.
20. Chai, J., Shiozaki, E., Srinivasula, S. M., Wu, Q., Datta, P., Alnemri, E. S., Shi, Y., and Dataa, P. (2001) *Cell 104*, 769−80.
21. Huang, Y., Park, Y. C., Rich, R. L., Segal, D., Myszka, D. G., and Wu, H. (2001) *Cell 104*, 781−90.
22. Riedl, S. J., Renatus, M., Schwarzenbacher, R., Zhou, Q., Sun, C., Fesik, S. W., Liddington, R. C., and Salvesen, G. S. (2001) *Cell 104*, 791−800.
23. Deveraux, Q. L., Leo, E., Stennicke, H. R., Welsh, K., Salvesen, G. S., and Reed, J. C. (1999) *EMBO J. 18*, 5242−51.
24. Sun, C., Cai, M., Meadows, R. P., Xu, N., Gunasekera, A. H., Herrmann, J., Wu, J. C., and Fesik, S. W. (2000) *J. Biol. Chem. 275*, 33777−81.
25. Srinivasula, S. M., Hegde, R., Saleh, A., Datta, P., Shiozaki, E., Chai, J., Lee, R. A., Robbins, P. D., Fernandes-Alnemri, T., Shi, Y., and Alnemri, E. S. (2001) *Nature 410*, 112−6.
26. Vucic, D., Deshayes, K., Ackerly, H., Pisabarro, M. T., Kadkhodayan, S., Fairbrother, W. J., and Dixit, V. M. (2002) *J. Biol. Chem. 277*, 12275−9.
27. Shiozaki, E. N., Chai, J., Rigotti, D. J., Riedl, S. J., Li, P., Srinivasula, S. M., Alnemri, E. S., Fairman, R., and Shi, Y. (2003) *Mol. Cell 11*, 519−27.
28. Du, C., Fang, M., Li, Y., Li, L., and Wang, X. (2000) *Cell 102*, 33−42.
29. Verhagen, A. M., Ekert, P. G., Pakusch, M., Silke, J., Connolly, L. M., Reid, G. E., Moritz, R. L., Simpson, R. J., and Vaux, D. L. (2000) *Cell 102*, 43−53.
30. Suzuki, Y., Imai, Y., Nakayama, H., Takahashi, K., Takio, K., and Takahashi, R. (2001) *Mol. Cell 8*, 613−21.
31. Hegde, R., Srinivasula, S. M., Zhang, Z., Wassell, R., Mukattash, R., Cilenti, L., DuBois, G., Lazebnik, Y., Zervos, A. S., Fernandes-Alnemri, T., and Alnemri, E. S. (2002) *J. Biol. Chem. 277*, 432−8.
32. Martins, L. M., Iaccarino, I., Tenev, T., Gschmeissner, S., Totty, N. F., Lemoine, N. R., Savopoulos, J., Gray, C. W., Creasy, C. L., Dingwall, C., and Downward, J. (2002) *J. Biol. Chem. 277*, 439−44.
33. Verhagen, A. M., Silke, J., Ekert, P. G., Pakusch, M., Kaufmann, H., Connolly, L. M., Day, C. L., Tikoo, A., Burke, R., Wrobel, C., Moritz, R. L., Simpson, R. J., and Vaux, D. L. (2002) *J. Biol. Chem. 277*, 445−54.
34. White, K., Grether, M. E., Abrams, J. M., Young, L., Farrell, K., and Steller, H. (1994) *Science 264*, 677−83.
35. Grether, M. E., Abrams, J. M., Agapite, J., White, K., and Steller, H. (1995) *Genes Dev. 9*, 1694−708.
36. Chen, P., Nordstrom, W., Gish, B., and Abrams, J. M. (1996) *Genes Dev. 10*, 1773−82.
37. Goyal, L., McCall, K., Agapite, J., Hartwieg, E., and Steller, H. (2000) *EMBO J. 19*, 589−97.
38. Srinivasula, S. M., Datta, P., Kobayashi, M., Wu, J. W., Fujioka, M., Hegde, R., Zhang, Z., Mukattash, R., Fernandes-Alnemri, T., Shi, Y., Jaynes, J. B., and Alnemri, E. S. (2002) *Curr. Biol. 12*, 125−30.
39. Wing, J. P., Karres, J. S., Ogdahl, J. L., Zhou, L., Schwartz, L. M., and Nambu, J. R. (2002) *Curr. Biol. 12*, 131−5.
40. Christich, A., Kauppila, S., Chen, P., Sogame, N., Ho, S. I., and Abrams, J. M. (2002) *Curr. Biol. 12*, 137−40.
41. Liu, Z., Sun, C., Olejniczak, E. T., Meadows, R. P., Betz, S. F., Oost, T., Herrmann, J., Wu, J. C., and Fesik, S. W. (2000) *Nature 408*, 1004−8.
42. Wu, G., Chai, J., Suber, T. L., Wu, J. W., Du, C., Wang, X., and Shi, Y. (2000) *Nature 408*, 1008−12.
43. Wu, J. W., Cocina, A. E., Chai, J., Hay, B. A., and Shi, Y. (2001) *Mol. Cell 8*, 95−104.
44. Silke, J., Hawkins, C. J., Ekert, P. G., Chew, J., Day, C. L., Pakusch, M., Verhagen, A. M., and Vaux, D. L. (2002) *J. Cell Biol. 157*, 115−24.
45. Kipp, R. A., Case, M. A., Wist, A. D., Cresson, C. M., Carrell, M., Griner, E., Wiita, A., Albiniak, P. A., Chai, J., Shi, Y., Semmelhack, M. F., and McLendon, G. L. (2002) *Biochemistry 41*, 7344−9.
46. Guo, F., Nimmanapalli, R., Paranawithana, S., Wittman, S., Griffin, D., Bali, P., O'Bryan, E., Fumero, C., Wang, H. G., and Bhalla, K. (2002) *Blood 99*, 3419−26.
47. Arnt, C. R., Chiorean, M. V., Heldebrant, M. P., Gores, G. J., and Kaufmann, S. H. (2002) *J. Biol. Chem. 277*, 44236−43.
48. Fulda, S., Wick, W., Weller, M., and Debatin, K. M. (2002) *Nat. Med. 8*, 808−15.
49. Sidhu, S. S., Lowman, H. B., Cunningham, B. C., and Wells, J. A. (2000) *Methods Enzymol. 328*, 333−63.
50. Nielsen, H., Engelbrecht, J., Brunak, S., and von Heijne, G. (1997) *Protein Eng. 10*, 1−6.
51. Deshayes, K., Schaffer, M. L., Skelton, N. J., Nakamura, G. R., Kadkhodayan, S., and Sidhu, S. S. (2002) *Chem. Biol. 9*, 495−505.
52. Keating, S. M., Marsters, J., Beresini, M., Ladner, C., Zioncheck, K., Clark, K., Arellano, F., and Bodary, S. (2000) in *Proceedings of SPIE: In Vitro Diagnostic Instrumentation* (Cohn, G. E., Ed.) pp 128−137, Bellingham, WA.
53. Otwinowski, Z., and Minor, W. (1997) *Methods Enzymol. 276*, 307−26.
54. Jones, T. A., Zou, J. Y., Cowan, S. W., and Kjeldgaard, M. (1991) *Acta Crystallogr. A47*, 110−9.
55. Collaborative Computational Project, Number 4 (1994) *Acta Crystallogr. D50*, 760−763.
56. Murshudov, G. N., Vagin, A. A., and Dodson, E. J. (1997) *Acta Crystallogr. D53*, 240−255.
57. Perrakis, A., Morris, R., and Lamzin, V. S. (1999) *Nat. Struct. Biol. 6*, 458−63.
58. Laskowski, R. A., MacArthur, M. W., Moss, D. S., and Thornton, J. M. (1993) *J. Appl. Crystallogr. 26*, 283−91.
59. LaCasse, E. C., Baird, S., Korneluk, R. G., and MacKenzie, A. E. (1998) *Oncogene 17*, 3247−59.
60. Tamm, I., Kornblau, S. M., Segall, H., Krajewski, S., Welsh, K., Kitada, S., Scudiero, D. A., Tudor, G., Qui, Y. H., Monks, A., Andreeff, M., and Reed, J. C. (2000) *Clin. Cancer Res. 6*, 1796−803.
61. DeLano, W. L. (2002) *The PyMOL Manual*, DeLano Scientific, San Carlos.

BI034227T